Made available for a limited time for personal research and study only License.

ACS APPLIED ENGINEERING MATERIALS

pubs.acs.org/acsaenm Article

Modified Graphene Oxide as an Additive to Enhance the Lubricity of the Ionic Liquid, 1-Heptyl-3-methylimidazolium Bis[(trifluoromethane)sulfonyl]amide

Sujoy Talukder, Jagdeep Kaur, Jeremy Lawerence, Jiahe Xu, Ramesh Dinesh Choudhary, Carol Korzeniewski, Edward L. Quitevis, and Chang-Dong Yeo*

Cite This: https://doi.org/10.1021/acsaenm.2c00177 Read Online

ACCESS | Metrics & More | Article Recommendations | Supporting Information

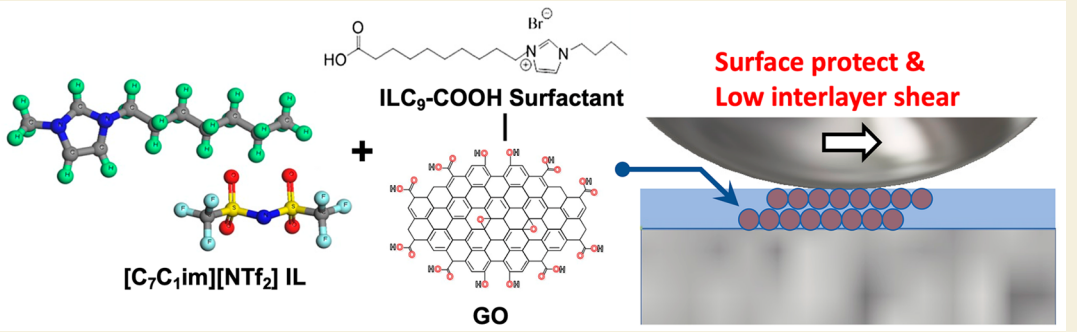

ABSTRACT: Nanocarbon products and graphene derivatives are often applied to base lubricants as an additive to reduce contact-induced surface failures and improve the reliability of engineering applications. In this study, the effects of modified graphene oxide (MGO) on the lubricity of the ionic liquid (IL), 1-heptyl-3-methyl imidazolium bis[(trifluoromethane)sulfonyl]amide ($[C_7C_1im][NTf_2]$), are investigated through systematic experiments and material characterizations. To enhance the stability of the dispersion of GO in the IL $[C_7C_1im][NTf_2]$ lubricant, 1-butyl-3-(9-carboxynonyl)imidazolium bromide (ILC_9-COOH) is covalently grafted onto GO, which produces ILC_9-COOH-modified graphene oxide (MGO). The synthesized MGO/IL lubricant is applied to the sliding contact between the stainless steel ball and the bearing steel plate. The measured friction and wear are analyzed with respect to the MGO concentration and temperature. The experimental results support that MGO is an effective additive to the IL $[C_7C_1im][NTf_2]$ lubricant in decreasing the friction, and its benefit is more obvious at the higher temperature. From the analysis of the 3D surface profilometer and scanning electron microscopy (SEM) measurements, it is found that the abrasive type of wear is dominant on the worn surface. If the MGO concentration is appropriately controlled, MGO additive can be beneficial in decreasing the wear at the higher temperature.

KEYWORDS: *ionic liquid, graphene derivative, additive, dispersion, friction, wear*

Downloaded via TEXAS TECH UNIV on January 29, 2023 at 00:42:17 (UTC).
See https://pubs.acs.org/sharingguidelines for options on how to legitimately share published articles.

1. INTRODUCTION

The presence of friction and wear on the contacting surface is one of the key issues in a transportation system affecting its fuel efficiency and performance.[1] Researchers have been working on new lubrication technologies to enhance fuel efficiency and extend the service life of machines, which is usually achieved by dissipating heat from contact interfaces, inhibiting corrosion like oxidative events, and removal of contaminants (foreign particle, oxidized product, etc.), along with minimizing friction and wear. In general, frictional heat is omnipresent at the rubbing contact interface, which changes the viscosity and promotes auto-oxidation of the lubricant at elevated temperatures. To address the design requirements of a lubrication system, various types of additives have been studied such as antiwear component, friction-modifier, corrosion-oxidation inhibitor, detergent, dispersant, and so on.[2]

Graphene and its derivatives (i.e., graphene oxide (GO) and reduced graphene oxide (RGO)) have been studied as an additive to lubricants.[3−7] Due to their superior thermal conductivity and low plane-shear resistance, they can improve the tribological performance of a surface-contact device.[3−5,8,9] When graphene particles are applied to a liquid lubricant, the dispersion quality is challenging because of the inherent chemical inertness and $\pi-\pi$ stacking interaction between

Received: October 21, 2022
Accepted: January 13, 2023

© XXXX American Chemical Society

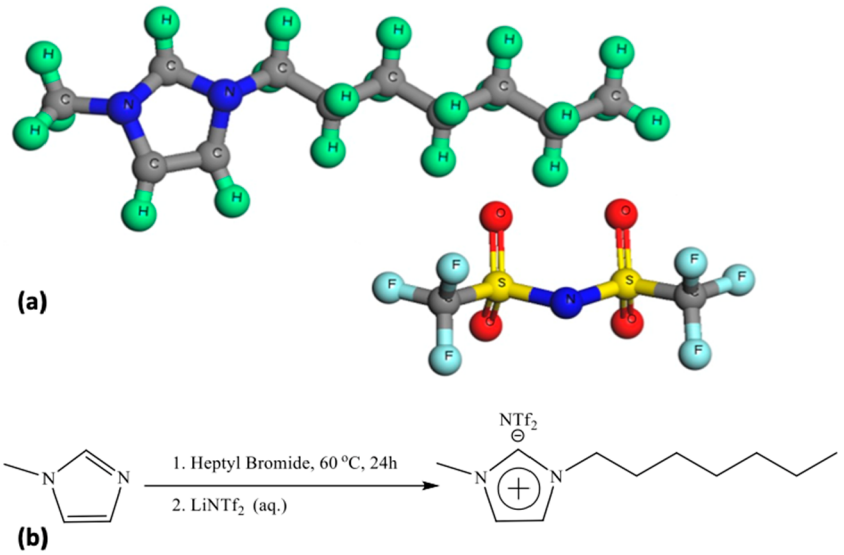

Figure 1. 1-Heptyl-3-methylimidazolium bis[(trifluoromethane)sulfonyl]amide, $[C_7C_1im][NTf_2]$: (a) molecular structure and (b) synthesis.

graphene sheets.[10] In the case of GO as an oxidized derivative of graphene, GO shows excellent dispersibility in polar solvents. The presence of oxygen rich groups (i.e., hydroxyl and epoxy) on the basal plane along with smaller fractions of carboxyl, carbonyl, and phenol groups at the sheet edges makes GO hydrophilic, which allows better interfacial interaction with polar solvents.[10] Compared to GO, reduced graphene oxide (RGO) contains a smaller number of oxygen functionalized groups, which accordingly reduces the polar interaction capacity, thereby preserving similar configuration and properties with pristine graphene.[11]

Ionic liquids (ILs) have been evaluated as an alternative or additive for high-performance synthetic lubricants.[12−38] ILs exhibit exceptional characteristics including high thermal stability, high polarity, low melting point, nonflammability, and negligible volatility, which make them an excellent candidate for lubricants compared to conventional oils and greases.[13−16] ILs are defined as organic salts with melting points below 100 °C. They are also referred to as room temperature ILs (RTILs) if their melting points are at or below room temperature. An IL is typically comprised of a large asymmetric organic cation and an inorganic anion. Due to the nature and structure of the ions involved, forming a regular crystalline structure is difficult in ILs, which make them liquids at room temperature.[17] When ILs are applied on a metal surface, the inorganic anions are anchored and strongly bonded to the exposed metal surface, while the cations form a layer over the anions, making an ordered layered structure.[18−20] These absorbed layered structures effectively prevent direct solid-to-solid contact at low contact load conditions. At higher contact load conditions, these layered structures can be broken and decomposed leading to tribochemical reactions with the metal by the local high contact stress and temperature rise, which can create a protective tribofilm on the metal surfaces, thereby reducing the friction and wear.[18,21,22]

Given that steel is a popular material in machines, researchers have investigated the properties of ILs as a lubricant for steel−steel contact.[18,20,22] Various types of anions and cations have been used to synthesize ILs to address a specific tribological performance.[18] It was observed that imidazolium-based ILs provide good thermal stability.[23] ILs with hydrophobic anions such as tetrafluoroborate ($[BF_4]^-$) and hexafluorophosphate ($[PF_6]^-$) cause a corrosion on the steel surface under humid conditions, whereas bis[tri-(fluoromethane)sulfonyl]amide ($[NTf_2]^-$) shows better thermo-oxidative stability and tribological performance.[18,24,25] It was also found that ILs with longer alkyl chains are beneficial for improving the friction of steel−steel contacts.[18]

Several nanomaterials such as nanodiamond, carbon black, and silicon nitride have been applied as an additive to IL lubricants, all of which helped to reduce the friction and wear of contacting solids.[26−28] Graphene has also been investigated as an additive to IL lubricants decreasing the friction and wear if its wt % is appropriately controlled.[28−31] To improve the dispersibility of graphene derivatives in base oils, its surface is modified using IL surfactant producing IL-functionalized graphene derivatives. Researchers have studied IL-functionalized graphene derivatives as an additive for various types of base lubricants such as synthetic oil, formulated oil, and deionized water[32−38] and found that these additives worked well as a wear inhibitor and friction reducer. However, there have been few works reported for IL-functionalized graphene derivatives as an additive for base IL lubricants.

In this study, the monocationic ionic liquid (MIL), 1-heptyl-3-methylimidazolium bis[(trifluoromethane)sulfonyl]amide ($[C_7C_1im][NTf_2]$), is synthesized as a base lubricant, while modified graphene oxide (MGO) is manufactured as an additive. The MGO/IL is applied to a steel−steel contact as a lubricant. Using a ball-on-flat linear reciprocating tribometer, its lubricity (i.e., friction and wear) is analyzed with respect to the concentration of MGO additive and the temperature. The wear mechanism and volume of the tested samples are analyzed using an optical 3-D profilometer and scanning electron microscopy (SEM). Compared to other related works, the unique feature of this study is the application of MGO as an additive for IL base lubricant and the measurements of its lubricity at a wider range of temperatures.

https://doi.org/10.1021/acsaenm.2c00177
ACS Appl. Eng. Mater. XXXX, XXX, XXX−XXX

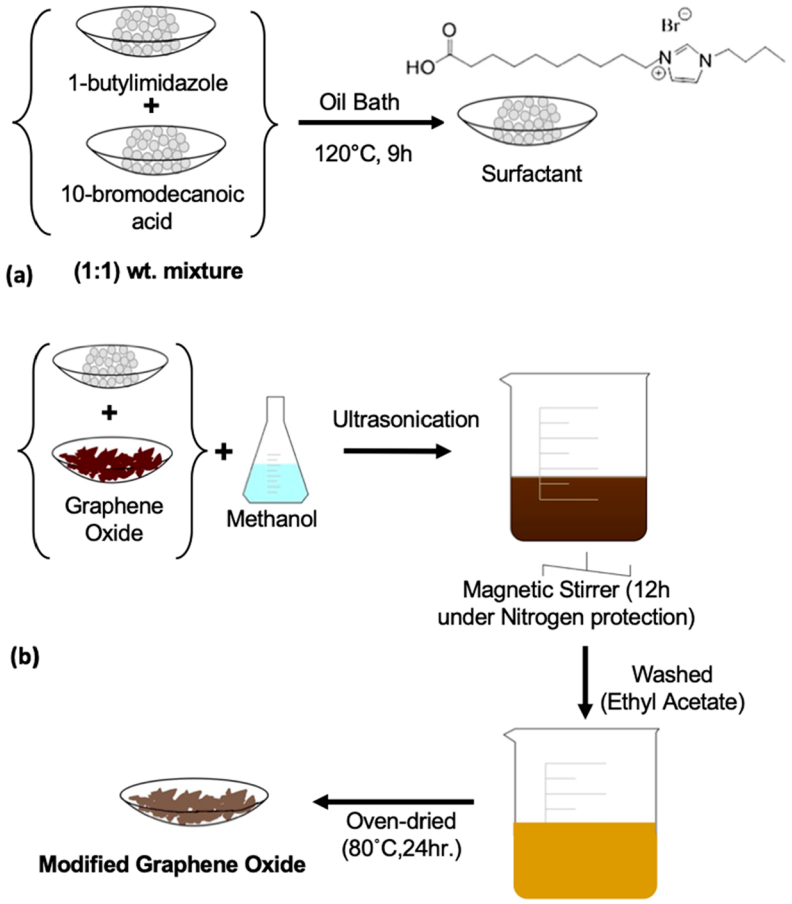

Figure 2. (a) Synthesis of surfactant ILC_9-COOH; (b) production of modified graphene oxide (MGO).

2. EXPERIMENTAL

2.1. Synthesis of the Ionic Liquid (IL) and Graphene Derivatives

Ionic Liquid (IL). The IL used in this study has an asymmetric imidazolium cation and $[NTf_2]^-$ as the anion as shown in Figure 1a. Its synthesis is a two-step process as schematically shown in Figure 1b. This procedure has been optimized by Quitevis and co-workers in their previous works.[39−41] A total of 1 equivalent of 1-methylimidazole and 1.05 equivalent of 1-bromoheptane were added to 50 mL of acetonitrile, and the solution was left to stir overnight at 60 °C under nitrogen. ^{1}H NMR showed that the crude product is the desired intermediate, $[C_7C_1im][Br]$, with slight impurities, confirming complete consumption of 1-methylimidazole. The reaction mixture was washed with 50 mL of a 3:1 (v/v) mixture of hexane and dichloromethane three times and left to stir in hexane at room temperature overnight to remove the unreacted halide. The product was concentrated in *vacuo* on a rotary evaporator. The resultant IL was used in the second step of the synthesis without further purification. The second step involved a metathesis reaction in which 1 equivalent of $[C_7C_1im][Br]$ and 0.97 equivalent of lithium bis[tri-(fluoromethane)sulfonyl]amide ($LiNTf_2$) were mixed in aqueous solution and left to stir overnight at room temperature. The two-phase system was then repeatedly washed with distilled water until no bromide ions were detected by the silver nitrate test. The excess water was removed by benzene azeotrope by using a Dean−Stark trap. The crude product was decolorized by stirring in activated carbon and acetonitrile for 96 h and then filtered through a gravitational column that was packed with glass wool, sand, 10 cm of aluminum oxide (activated, basic, 50−200 μm), and 5 cm of Celite 545 and again sand on the top, using acetonitrile as the eluent. After removal of the solvent using a rotary evaporator under the reduced pressure, a colorless liquid of $[C_7C_1im][NTf_2]$ was formed. The complete drying and removal of residual benzene was carried under vacuum at 70 °C, which was confirmed by measuring water content (below 100 ppm) using Karl Fischer titration. The final purity of the IL was confirmed by ^{1}H NMR (see Figure S1 and NMR data in the Supporting Information). Quitevis and co-workers previously showed the procedure for the synthesis and purification described above yields an IL with purity >99% as confirmed by elemental analysis and electrospray ionization mass spectrometry.[41]

Graphene Oxide (GO) and Reduced Graphene Oxide (RGO). Using the modified Hummer's method,[42] GO and RGO were synthesized following the procedures illustrated in Figure S3 and S4 in the Supporting Information. To obtain GO, 180 mL of sulfuric acid (H_2SO_4, 98%) was mixed with 20 mL of phosphoric acid (H_3PO_4) with a 9:1 volume ratio and left to stir for 15 min. A total of 1.5 g of graphite powder was added to the acid solution, followed by the slow addition of 9.0 g of $KMnO_4$ with continuous stirring. The mixture was left to stir continuously for 72 h to allow enough time for the graphite to be oxidized in the presence of $KMnO_4$. A total of 4 mL of hydrogen peroxide (H_2O_2, 30%) was then added to terminate the oxidation reaction. Upon successful oxidation, the solution

https://doi.org/10.1021/acsaenm.2c00177
ACS Appl. Eng. Mater. XXXX, XXX, XXX−XXX

turned golden-yellow in color. After confirming the color change, the solution was rigorously washed with deionized (DI) water and hydrochloric acid (HCl, 30%) and again with DI water. The solution was then centrifuged at 4,500 rpm until the pH became neutral (approximately 10 min). After the centrifugation, the supernatant was oven-dried at 45 °C for 24 h to produce GO.

RGO was obtained through the exfoliation of GO via a stepwise increase in temperature.[43] The oven-dried GO obtained via the synthetic process (Figure S3 in the Supporting Information) was exfoliated with DI water using ultrasonication. The mixture was oven-dried with the temperature increments of 25 °C at every 10 min until reaching 300 °C in 2 h. This procedure eliminates most of the oxygen functional groups in GO to produce RGO.

Modified Graphene Oxide (MGO). As an additive to IL lubricants, GO has a critical issue of bad dispersibility. To improve its dispersibility, surface modification was conducted using a surfactant. In this study, the surfactant, 1-butyl-3-(9-carboxynonyl)imidazolium bromide (ILC_9-COOH), was synthesized by heating a 1:1 molar ratio of 1-butylimidazole and 10-bromodecanoic acid in an oil bath at 120 °C for 9 h, as shown in Figure 2a.[44] The purity of the surfactant was confirmed by ^{1}H NMR (see Figure S2 and NMR data in the Supporting Information). Based on the technique developed by He et al.,[45] MGO could be obtained following the procedure outlined in Figure 2b. A 1:1 (w/w) ratio of GO and the surfactant ILC_9-COOH were mixed with methanol via ultrasonication for 1 h. The mixture was stirred for 12 h under nitrogen at room temperature to ensure complete reaction. Ethyl acetate was used to wash the solution to remove excess surfactant. The solution was oven-dried at 80 °C for 24 h, which produced ILC_9-COOH modified graphene oxide MGO.

2.2. Material Characterization

Viscosity Measurements. The viscosities of the pure IL $[C_7C_1im][NTf_2]$ and the MGO/IL lubricant were measured as a function of temperature using a TA Instruments Discovery HR-3 rheometer and a double-wall concentric cylinder Couette cell with shear rates varying from 10 to 1000 s^{-1}. The viscosity was measured from 298.15 to 373.15 K for the 0.1 wt % MGO/IL lubricant, while it was measured at 298.15 and 373.15K for the IL. (The viscosities of the IL and 0.1 wt % MGO/IL lubricant are listed in Table S1 of the Supporting Information.) Figure 3 shows the viscosities of the IL and 0.1 wt % MGO/IL lubricant plotted as a function of temperature, as well as the viscosity of the IL obtained from a previous study.[46] The dashed lines through the data are fits of the Vogel−Fulcher−Tammann (VFT) equation:[47,48]

$$\eta = \eta_0 \exp\left(\frac{B}{T - T_0}\right) \quad (1)$$

where parameters η_0, B, and T_0 are given in Table S2 in the Supporting Information.

From the results in Figure 3, the values of the viscosity of the IL obtained in the current study at 298.15 and 373.15 K are in good agreement with the values obtained by Xue et al.[46] within the ±2 mPa·s experimental error of the measurements. This provides support for the comparison between the viscosity of the IL obtained by Xue et al.[46] and that of MGO/IL obtained in the current study being valid. The plot as well as Table S3 in the Supporting Information indicate the viscosity of 0.1 wt % MGO/IL is lower than that of the neat IL. Based on the fits of

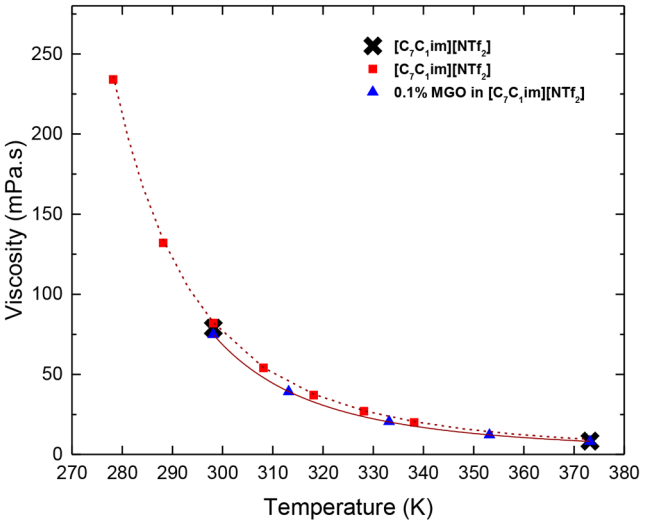

Figure 3. Comparison of viscosity values of neat $[C_7C_1im][NTf_2]$ from the current study (× points) and literature values from Xue et al.[46] (square points) and 0.1 wt % MGO/$[C_7C_1im][NTf_2]$ lubricant (triangle points). Dashed and solid lines correspond to fits of the VFT equation (eq 1) to the viscosity values.

VFT equation to the viscosities of MGO/IL and the neat IL, this difference holds outside the region of measured viscosities. These results indicate adding MGO to the IL lowers the viscosity by at most 13% (see Table S3 in Supporting Information).

Thermal Gravimetric Analysis (TGA). The thermal stabilities of the IL and the 0.1 wt % MGO/IL lubricant were examined using a Shimadzu DTG-60H thermogravimetric analyzer under ambient air with a controlled flow rate of 10 mL/min. An empty alumina pan was used as the reference and a second alumina pan was used as the sample holder. The weights of the samples ranged from 5 to 10 mg. Two measurements were done on each sample using the dynamic method where the samples were heated from 25 to 600 °C. The onset temperature, T_{onset}, corresponding to the intersection of the zero-mass loss baseline and the tangent line of mass loss, and the 10% mass loss temperature $T_{10\%}$ are given in Table S4 in the Supporting Information.

The dynamic TGA curves at 10 K/min for the IL and the 0.1 wt % MGO/IL lubricant are shown in Figure 4. For the neat IL the values of T_{onset} for the 2 runs were 404 and 405 °C, whereas for the 0.1 wt % MGO/IL lubricant the values of T_{onset} for the 2 runs were 395 and 398 °C, indicating that the thermal stability of neat IL is greater than that of the 0.1 wt % MGO/IL lubricant by 8 °C. This result is also consistent with values of $T_{10\%}$ being greater for IL (387 °C for both runs) than for the 0.1 wt % MGO/IL lubricant (382 and 387 °C). Based on TGA, both the IL and the 0.1 wt % MGO/IL should be thermally stable during the friction and wear measurements performed at elevated temperature of 100 °C.

XRD, SEM, and FTIR of the Synthesized Graphene Derivatives. The synthesized GO, RGO, and MGO were characterized using X-ray diffraction (XRD), scanning electron microscopy (SEM), and Fourier transform infrared (FTIR) spectroscopy. The XRD spectra of graphite, GO, and RGO, which were obtained using Rigaku Ultima III in the range of 2θ from 5° to 60°, are shown in Figure 5. The XRD spectrum of graphite (gray) has a very narrow-intense peak at a 2θ of 26.21°. This peak corresponds to the (002) planes of the

https://doi.org/10.1021/acsaenm.2c00177
ACS Appl. Eng. Mater. XXXX, XXX, XXX−XXX

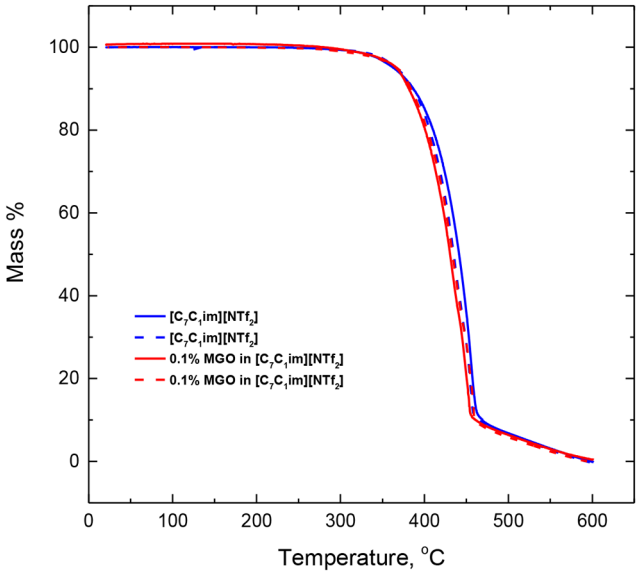

Figure 4. TGA thermogram for $[C_7C_1im][NTf_2]$ (blue lines) and for 0.1 wt % MGO in $[C_7C_1im][NTf_2]$ (red lines). The solid and dashed lines for the IL and MGO/IL lubricant correspond to two different runs.

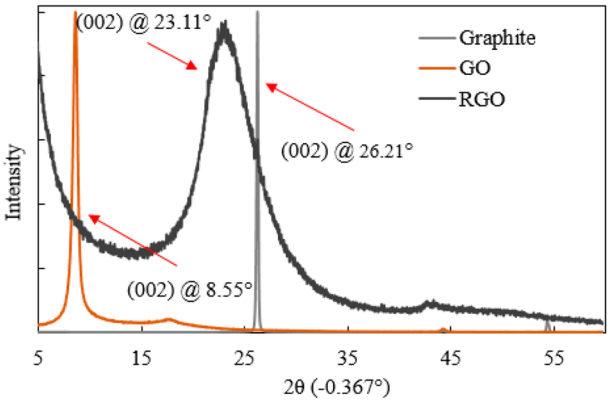

Figure 5. XRD spectra for graphite, GO, and RGO.

graphene layers. However, the XRD spectrum of GO (brown) shows a narrow-intense peak at 2θ of 8.55°. During the oxidation process, the graphite structure expands because oxygen-containing groups are incorporated between the carbon layers. Due to this structural change, the narrow-intense peak of GO is shifted far from the graphite peak. In the case of RGO, as the oxygen-containing groups are eliminated following the process in Figure S4 in the Supporting Information, a narrow-intense peak is observed at 2θ = 23.11° close to the graphite peak.[49,50]

SEM images for the bulk GO and MGO samples shown in Figure 6 were obtained using a Zeiss Crossbeam 540 FIB-SEM at 1K, 3K, and 10K times magnifications. The SEM images show striking differences in the surface morphologies of GO and MGO. At 1 K magnification, SEM images show the surface of GO to be continuous and that of MGO to be disordered. At 3 K magnification, the SEM images show the surface of GO to be comprised of overlapping, slightly wrinkled layers on the order of 20−30 μm in size whereas that of MGO to be comprised of roughly shaped fragments, with some less than 10 μm in size.

The FTIR spectra for graphite, GO, ILC_9-COOH, and MGO, shown in Figure 7 were obtained using a Thermo Scientific iS5 FTIR spectrometer with the high performance iD7 ATR accessory. The spectrum of graphite is smooth, lacking any spectral features. In contrast, the spectrum of GO which results from the oxidation of graphite by strong mineral acids with strong oxidizing agents such as in the Hummer process has many vibrational bands associated with aromatic regions with nonoxidized rings and regions with aliphatic six-membered rings with oxygen functionalities such a 1,2-epoxides and hydroxyl groups in the basal-plane and carbonyl, carboxyl, and hydroxyl groups at the edges. For example, the 1148 and 1387 cm^{-1} bands correspond to the epoxy (C−O−C) stretching mode located over the basal plane of GO; the 1251 and 1714 cm^{-1} bands correspond, respectively, to phenol-related (C−OH) groups and carboxyl (−COOH) groups located on the edge of the GO sheets; and the 953 and 1624 cm^{-1} bands correspond to the C═C vibrations of the graphene skeleton. The broad band between 3300 and 2500 cm^{-1} corresponds to the O−H stretch. Superimposed on the O−H band are intense bands at 2980 and 2882 cm^{-1} corresponding to C−H vibrations associated with the aliphatic six-membered rings with oxygen functionalities.[51]

As one would expect given its molecular structure, the FTIR spectrum of ILC_9-COOH is complex. Despite its complexity, there are several vibrational bands that can be assigned to functional groups in this surfactant. For example, the carboxyl OH stretch is a very broad band in the region 3300−2500 cm^{-1} centered at ∼3000 cm^{-1}. Superimposed on the OH band are sharp bands in the 2900−2800 cm^{-1} region which are associated with the C−H vibrations corresponding the CH_3 and CH_2 groups in the butyl and nonyl chains in ILC_9-COOH, as well the aliphatic six-membered rings in the basal plane of GO.

In the case of the spectrum of MGO, the bands are due to oxygen functional groups on graphite layers but also bands due to the surfactant, ILC_9-COOH.[45] ILC_9-COOH is assumed to be covalently linked to the GO flakes via an esterification reaction between the carboxyl group of the surfactant and the OH groups on GO. Figure 8 shows a comparison of the spectra of MGO and ILC_9-COOH in the 2000−500 cm^{-1} spectral fingerprint region. Common to both spectra are strong bands at 1724 and 1708 cm^{-1} associated with the C═O stretching in MGO and ILC_9-COOH, respectively. Clearly, the presence of the strong C═O stretching band in these spectra indicates that GO has been modified. Despite the spectral congestion in this region, there are groups of bands that allow us to determine how the surfactant is bonded to GO. The region of 1440−750 cm^{-1} is unique to the carboxyl group, where bands at 1400 and 846 cm^{-1} are attributed to bending vibrations of OH and the band at 1166 cm^{-1} is attributed to a C−O stretching vibration. Upon esterification these OH bands disappear and are replaced by aromatic ester bands, which typically occur in the 1330−1000 cm^{-1} region and are associated with C−O stretching.

Raman Spectra of the GO and MGO. To understand the effect of grafting the surfactant IL onto GO, the Raman spectra of GO and MGO were recorded using a Raman microscope as described previously.[52,53] A brief description of the Raman microscope and analysis of the spectra is described in the Supporting Information.

Figure 9 shows the Raman spectra of GO and MGO. The D (1325−1336 cm^{-1}) and G (1600 cm^{-1}) bands as typical

https://doi.org/10.1021/acsaenm.2c00177
ACS Appl. Eng. Mater. XXXX, XXX, XXX−XXX

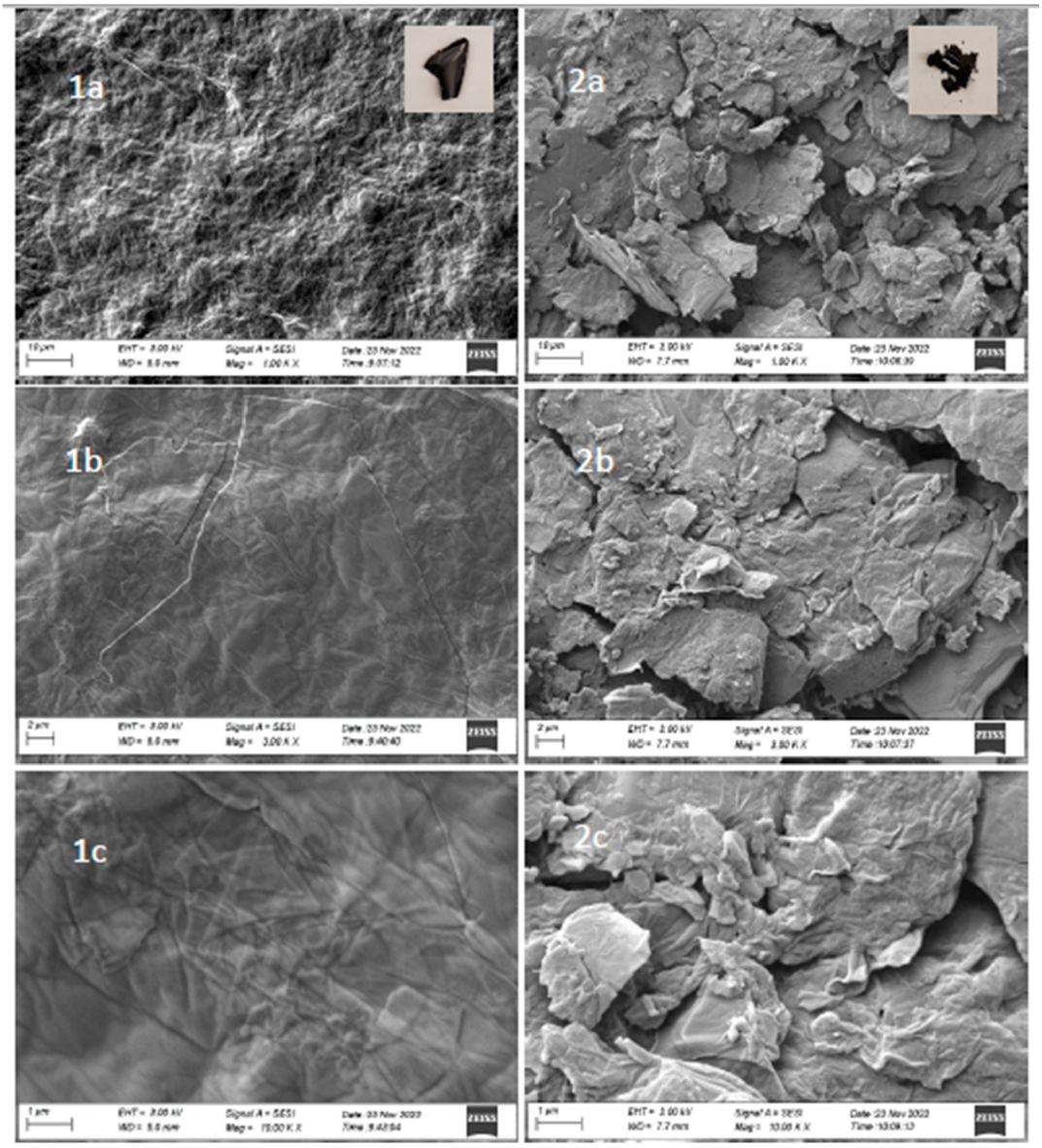

Figure 6. SEM images of GO (1a−c) and MGO (2a−c) at 1K, 3K, and 10K magnification. The bars indicating the scales of the images at these magnifications are, respectively, 10 μm, 2 μm, and 1 μm.

characteristics of carbon materials are evident.[54] The intensity of the D-band relative to that of the G-band is commonly used as a measure of the quality of graphene and graphene derivatives, reflecting the disorder due to edges, ripples, and defects, such as organic dopants. Compared to the spectrum of pristine GO, the greater breadth of features in the spectrum of the MGO sample indicates an increased degree of disorder in the processed material.[55]

The degree of disorder can be better quantified by deconvolving the spectra into component bands, G, D, D*, D′, and D″ as shown in Figure 9, where the D, D*, D′, and D″ bands correspond to various types of defects.[55] The D-band has been associated with breathing modes in the C−C ring structure, whereas the G-band is a Raman mode associated with $C(sp^2)-C(sp^2)$ bond stretching vibrations and therefore the graphitic structure. An increase in the ratio of intensity of the D*-component band to that of the G-component band is associated with an increase in the number of sp^3 bonds. Also increasing the contribution of the D″-component band to the spectrum, which leads to the broad shoulder between to two main features in spectrum of MGO, is associated with decreased crystallinity.[56] Table S5 in the Supporting Information gives the relative areas of these various component bands.

Interestingly, the area of the D-component band relative to that of the G-component band (see Table S4), A_D/A_G, is equal to 3.78 in the case of MGO, whereas it is equal to 5.00 in the case GO. This difference in the values of A_D/A_G seemingly suggests the degree of disorder of MGO is lower than that of GO, which is counterintuitive, if one assumes that grafting of the surfactant IL onto GO leads to increase in defects and disorder. However, the D-component band is associated with a specific defect that is correlated to breathing modes in the C−C ring. A more accurate reflection of the defects and disorder is given by the sum of the contributions of the D, D″, D′, and D* component bands relative to that of the G-component band, i.e., $(A_D + A_{D''} + A_{D'} + A_{D*})/A_G$. This ratio is equal to 5.25 in the case of MGO and equal to 5.59 GO, which suggests that the effect of grafting the surfactant IL onto GO is to distribute

https://doi.org/10.1021/acsaenm.2c00177
ACS Appl. Eng. Mater. XXXX, XXX, XXX−XXX

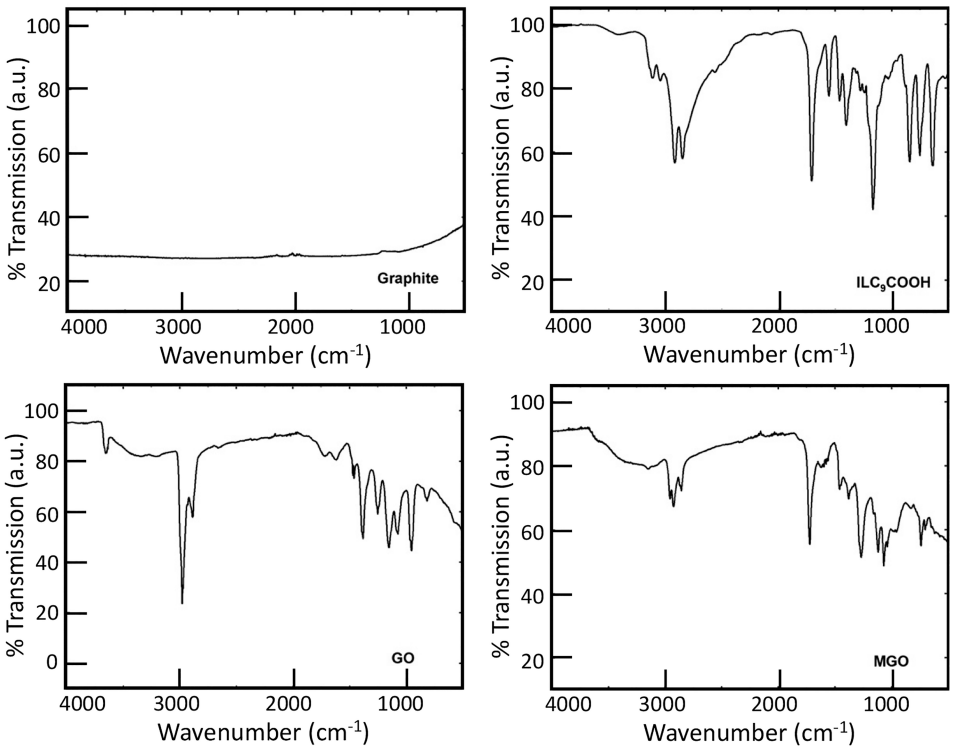

Figure 7. FTIR spectra for graphite, GO, ILC_9-COOH, and MGO.

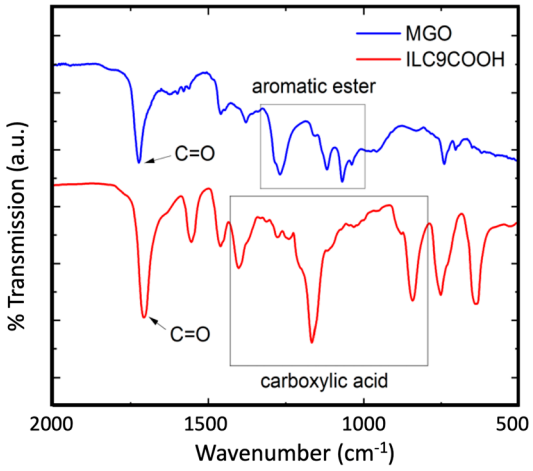

Figure 8. FTIR spectra of ILC_9-COOH and MGO in the 2000−500 cm^{-1} fingerprint region. The spectra are shifted vertically from their original positions to show more clearly the characteristic bands of the carbonyl and ester groups.

the defects in GO to other types of defects in MGO. For example, if one considers the D″-component band, the area ratio $A_{D''}/A_G$ is equal to 0.895 in the case of MGO and equal to 0.559 in the case of GO, which suggests an increase of disorder due to grafting of the surfactant IL onto GO. Moreover, if one considers the D*-component band, the area ratio A_{D*}/A_G is equal to 0.0824 in the case of MGO versus 0.0132 in the case of GO. This suggests an increase in the number of sp^3 bonds, which is consistent with grafting of the surfactant IL to GO.

Changes linked to increasing D-band prominence have also been observed in Raman spectra after IL processing of GO and associated with IL grafting at GO edge sites.[55,57] Ryu et al.[57] additionally observed a slight (∼6 cm^{-1}) downshift in the G band peak following grafting of alkylamine moieties to GO. The peak analysis in Table S5 reveals a similar downshift of ∼8 cm^{-1} following grafting of the surfactant IL onto GO.

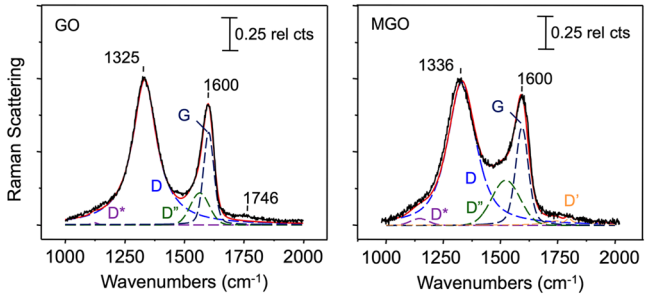

Figure 9. Raman spectra of GO and MGO with component bands obtained from deconvolution of the spectra.

Stability of GO/IL and MGO/IL Lubricants. To test the relative stability of GO/IL and MGO/IL lubricants, 0.1 wt % concentration of GO and MGO was prepared by sonicating capped vials containing 0.003 g of GO or MGO in 3 g of the IL for 1 h. Figure S5 in the Supporting Information shows pictures of the samples 0, 1, 2, and 5 h after sonication. MGO/IL is a better dispersed mixture as compared to GO/IL and remains well dispersed even after 5 h as indicated by the MGO/IL sample being a uniformly black dispersion, whereas the GO/IL sample being slightly discolored with particles of GO present at the bottom of the vial. To quantitatively confirm these visual images of the dispersions, the turbidity of the dispersions was determined by measuring the apparent absorbance of the dispersions relative to that of the pure IL at 600 nm by using UV−vis spectroscopy as a function of time for 300 min after sonication. Because GO and MGO have no absorbance at this wavelength,[58] the apparent absorbance

https://doi.org/10.1021/acsaenm.2c00177
ACS Appl. Eng. Mater. XXXX, XXX, XXX−XXX

should originate from light scattering from the suspended GO or MGO particles. Figure S6 in the Supporting Information shows that the turbidity of the MGO/IL dispersion is ~4.5 times that of the GO/IL dispersion, which is consistent with the MGO/IL sample being a better dispersed mixture compared to the GO/IL sample. Moreover, the turbidity of the mixtures showed no significant decrease during the period of the measurement. We conclude from this test that the MGO/IL lubricant is stable during the hour-long wear-friction measurements.

2.3. Experimental Methods for Friction and Wear Measurement

As GO and RGO have a low dispersion quality with the IL $[C_7C_1im][NTf_2]$, MGO was used as its additive. The friction and wear of MGO/IL lubrication system was evaluated using a ball-on-flat linear reciprocating tribometer as shown in Figure 10 (see ref 62 for further details).

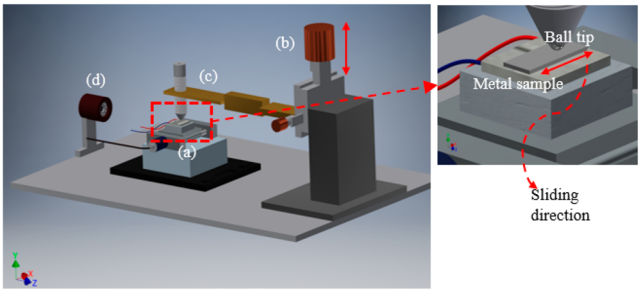

Figure 10. Ball-on-flat linear reciprocating tribometer: (a) temperature controllable motorized linear sample stage, (b) microstage to adjust the normal load, (c) tip holder and cantilever with two strain gauges, and (d) high resolution digital camera.[62]

The lower flat sample is made of bearing steel (AISI 52100), and the upper tip is a 440C stainless steel ball with a diameter of 4.8 mm. To minimize the effects of initial surface topography on the resulting friction and wear, the flat bearing steel was precisely polished using Knuth Rotor from Struers and sandpapers of grit size 320, 400, 800, 1500, and 3000, which provided a consistent surface roughness, i.e., root-mean-square (rms) roughness of ~20 nm. Under the contact load of 200 gf (= 1.96 N, producing the nominal contact pressure of 623 MPa), the linear sliding speed was set to 5 mm/s with the stroke of 5 mm. From the viscosity of applying lubricants (Table 3S in Supporting Information) and contact parameters, the Stribeck (or Hersey) number was calculated to be $4.47 \times 10^{-8} \sim 8.20 \times 10^{-7}$. This indicates that the lubrication regime in this experiment is boundary lubrication. The detailed information on the contact load selection and the resulting lubrication regime are found in the Supporting Information.

The bidirectional strain gauge system on the cantilever measures the in situ forces in normal and tangential (friction) directions. The sample temperature was controlled from room temperature (RT) to 100 °C under the relative humidity (RH) < 30%. It is noted that as conventional lubricants typically start their thermal degradation at the temperature of 100 °C ~ 200 °C,[59−61] we selected 100 °C as the comparing high temperature to RT. As an additive to the IL $[C_7C_1im][NTf_2]$ lubricant, the concentration of MGO was varied from 0 to 0.5 wt %. Before the lubricated contact test, the mixture of IL and MGO was ultrasonicated for 1 h at room temperature to generate a uniform and satisfactory dispersion. Based on the experimental design matrix in Table 1, the friction and wear performance of the MGO/IL lubricant was analyzed with respect to the concentration of MGO and temperature. For each set of experimental conditions, three repeated tests were performed at different locations to enable statistical analysis. After finishing each set of experiments, the surface wear of the flat bearing steel sample was quantified using a 3-D surface profilometer (Bruker Contour GT surface profiler), while the wear mechanisms were determined by SEM measurements. The more detailed information on the tribometer and experimental procedure are provided in Figure S7 in the Supporting Information.

Table 1. Experiment Design Matrix with the Variable of the Concentration of MGO and Temperature

Lubricant	Temperature	MGO
IL	RT	0
IL	RT	0.1 wt %
IL	RT	0.5 wt %
IL	100 °C	0
IL	100 °C	0.1 wt %
IL	100 °C	0.5 wt %

3. RESULTS AND DISCUSSION

3.1. Coefficient of Friction (COF) of the IL with Respect to MGO Concentration and Temperature

Figure 11 summarizes the measured COF values with elapsed contact time. First, as shown in Figure 11a, the IL lubricant without MGO additive (black solid line, black open square marker) showed a gradual increase in the COF value with elapsed time from 0.094 to 0.101 at room temperature. When 0.1 wt % MGO was applied to the IL as an additive, the 0.1 wt % MGO/IL lubricant (black dotted line, black open circle marker) showed a smaller COF value than the one from IL without MGO. The COF value slightly increased in the beginning of contact but quickly stabilized and saturated to a value of ~0.087. The MGO flakes in the IL can carry out two roles at the interface. First, they can be placed in between the two contacting surfaces preventing the direct solid−solid contact. Then, the smaller interlayer shear of the MGO flakes can produce less tangential force resulting in lower COF. Second, the MGO flakes at the interface can act as a third-body particle, which may have a negative impact on the friction, producing abrasive types of wear. Therefore, at the room temperature with 0.1 wt % MGO additive, the COF reduction by MGO's interlayer shear would be more dominant than the COF increase by the third-body abrasion, which could lead to the lower COF. When the MGO concentration increased to 0.5 wt % (black dashed line, black open triangle marker), it showed a smaller COF than the IL without MGO additive but higher COF than the IL with 0.1 wt % MGO. This implies that, with the excess amount of MGO additive, the contribution of the third-body abrasion might increase, which could result in the limited improvement of COF by MGO. The increase of the third-body abrasion at the 0.5 wt % MGO can be evidenced by the wear volume measurement in Figure 13. From the COF data in Figure 11a, it could be found that not only inclusion of MGO into the IL lubricant is effective to reduce the COF, but it also produces less variation in the COF values with elapsed contact time.

https://doi.org/10.1021/acsaenm.2c00177
ACS Appl. Eng. Mater. XXXX, XXX, XXX−XXX

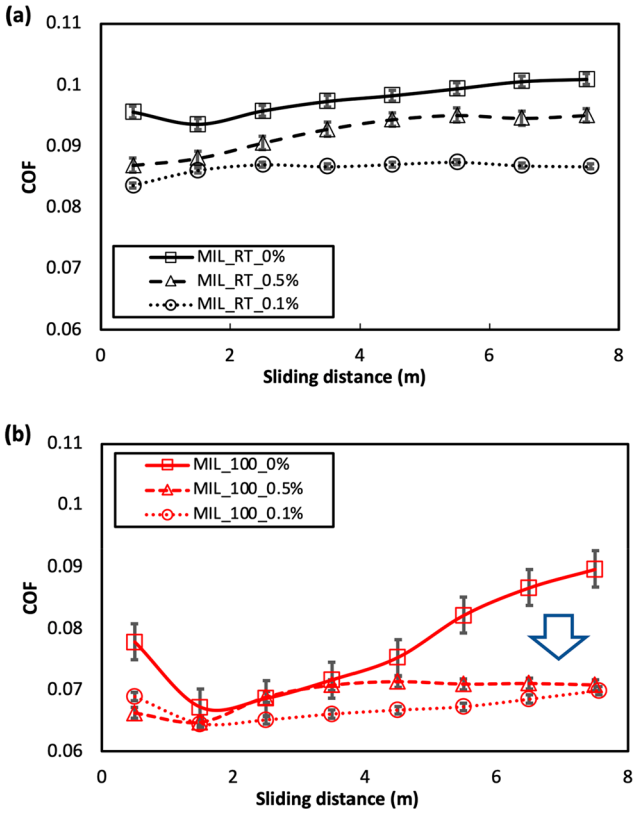

Figure 11. Measured COF values with the elapsed contact time at (a) room temperature and (b) high temperature of 100 °C. The error bars are the standard deviation of the measured COF values.

At the higher temperature of 100 °C, the value of COF (Figure 11b) was lower than the value of COF at room temperature (Figure 11a) due to the favorable tribofilm formed on the steel surfaces.[62−65] At boundary lubrication, the IL and MGO at the interface can make chemical reactions with the steel, forming a tribofilm on the surfaces that favorably reduces the friction, which is promoted at the higher temperature. In Figure 11b, the COF value decreased in the beginning of contact, which could be attributed to the run-in behavior of the contacting surfaces. Then, the IL lubricant without MGO additive (red solid line, red open square marker) showed an increasing trend of COF with the sliding distance from 0.065 to 0.090. Considering the IL lubricant film becomes thinner at higher temperature, the stainless-steel ball and the flat bearing steel can develop more solid−solid contacts causing the surface wear, which accordingly can increase the COF with elapsed contact time. When 0.1 wt % MGO was applied to the IL as an additive, the MGO/IL lubricant (red dotted line, red open circle marker) showed a smaller COF value than the one with IL without MGO. Despite the thinner lubricant film at the higher temperature, the value of COF at the higher temperature was stable with limited variation with elapsed contact time just like the value of COF at room temperature. For the case of MGO concentration of 0.5 wt % (red dashed line, red open triangle marker), the COF is slightly higher than the value with 0.1 wt % MGO, but the difference is statistically insignificant. This indicates that, in spite of the increased amount of MGO additive, the MGO flakes at the interface might be still beneficial to decrease the COF due to the limited work of third-body abrasion at the higher temperature of 100 °C.

These experimental results therefore strongly support that MGO is an effective additive to the IL $[C_7C_1im][NTf_2]$ lubricant in decreasing the friction of the steel−steel contact, and its benefit is more obvious at the higher temperature. It should be noted that to achieve the expected lubricity of MGO/IL lubricant, the amount of MGO additive may need to be adaptively controlled depending on system parameters such as materials, contact load/speed, operating temperature, and so on.

3.2. Surface Wear with Respect to MGO Concentration and Temperature

The wear of the postexperiment bearing-steel sample was quantified using the 3D surface profilometer (Contour GT by Bruker). Figure 12 shows representative wear tracks formed on the bearing steel surface after the sliding contact experiments. From the qualitative comparison of wear track images, it seems to show that the inclusion of MGO increases the surface wear at room temperature, but it does not significantly change the surface wear at 100 °C.

In this study, the 3-D surface scanning function in the Contour GT enabled the quantitative calculation of the wear volume of the bearing steel sample by comparing the wear track profile to the noncontact area. Figure 13 summarizes the

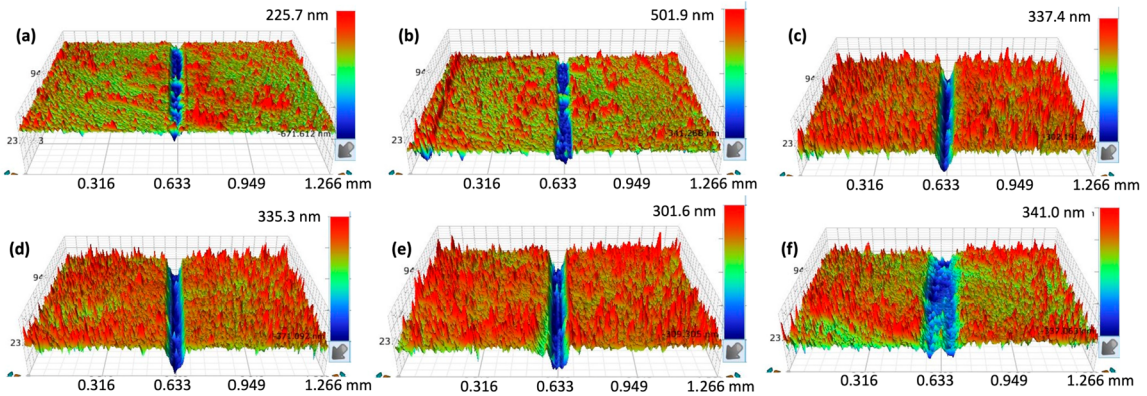

Figure 12. Wear track formed on the bearing streel sample after the experiment: At room temperature, (a) IL without MGO, (b) IL with 0.1 wt % MGO, and (c) IL with 0.5 wt % MGO. At 100 °C, (d) IL without MGO, (e) IL with 0.1 wt % MGO, and (f) IL with 0.5 wt % MGO. The images were measured using the Bruker Contour GT Profilometer.

https://doi.org/10.1021/acsaenm.2c00177
ACS Appl. Eng. Mater. XXXX, XXX, XXX−XXX

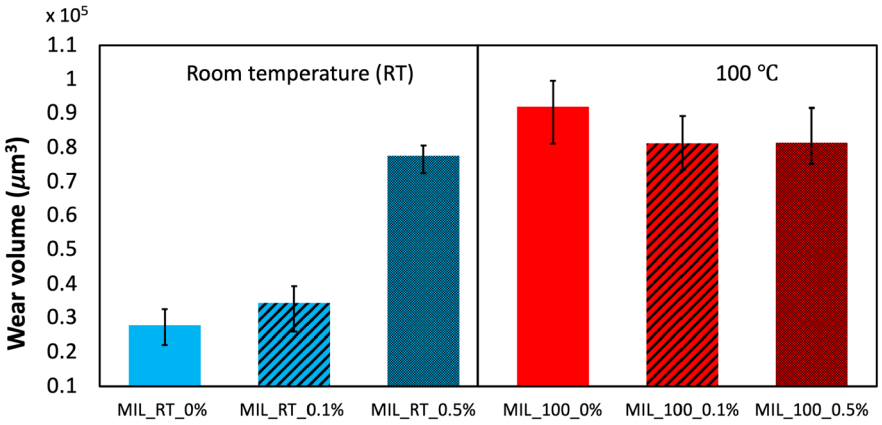

Figure 13. Wear volume comparison with respect to the MGO concentration and temperature.

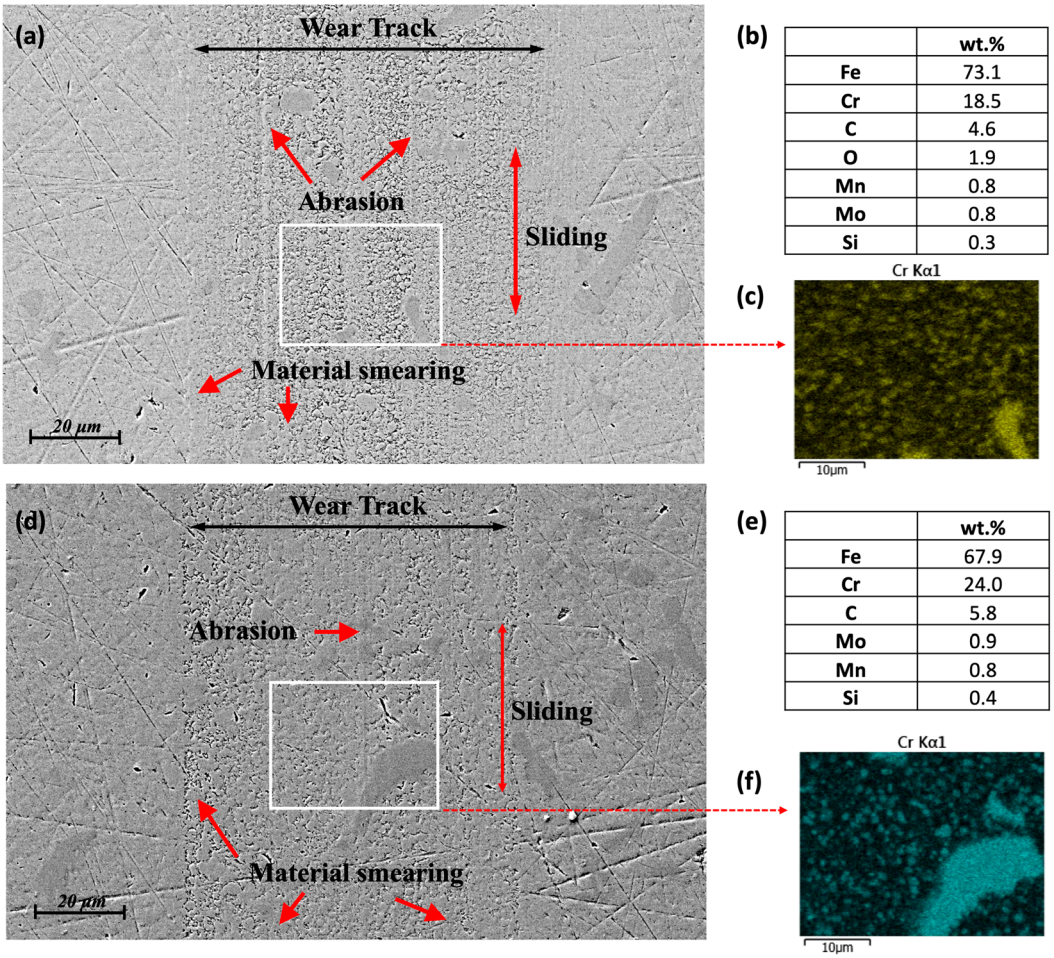

Figure 14. SEM and EDS analysis of the bearing steel surface after experiments at room temperature: (a–c) for the IL without MGO (neat IL) and (d–f) for the IL with 0.1 wt % MGO. (a) and (c) are SEM (SE mode) images, (b) and (e) are EDS data, and (c) and (f) are the element mapping images for Cr using backscattered electron (BSE) images.

measured wear volume with respect to the MGO concentration and temperature. At room temperature (RT), the inclusion of 0.1 wt % MGO in the IL as an additive did not significantly change the wear volume compared to the wear volume for the IL without MGO additive. However, when the MGO additive was increased to 0.5 wt %, it significantly increased the surface wear. This change of wear volume with the MGO concentration can be explained by the physical role of MGO during the surface contact. As discussed in Section 3.1, not only can MGO flakes at the interface prevent the direct solid–solid contact (reducing wear), but they can also produce a third-body abrasive wear (increasing wear). Therefore, if an excessive amount of MGO additive is applied in the IL, the contribution of the third-body abrasion can be more dominant at room temperature, which can negatively

https://doi.org/10.1021/acsaenm.2c00177
ACS Appl. Eng. Mater. XXXX, XXX, XXX–XXX

impact the tribological performance, increasing both friction and wear.

Next, at the higher temperature of 100 °C, first it was found that the wear volume increased by more than a factor of 3 compared to the wear volume at room temperature. This could be attributed to the more direct solid−solid contacts because of the thinner IL lubricant film at the interface. The inclusion of MGO in the IL produced smaller wear volume than the IL without MGO additive. Even though the difference of wear volumes is statistically insignificant, it implies that the MGO flakes in the IL might be working more as a wear inhibitor at the higher temperature. Because of the thinner IL lubricant film at 100 °C, the interface might have limited room for the MGO flakes to act a third-body particle, which could result in the lower wear volume.

The wear mechanism of the bearing steel sample was characterized using SEM/EDS measurement. Figure 14 compares the wear track formed on the bearing steel surface obtained from the IL without MGO additive (Figure 14a−c) and with 0.1 wt % of MGO additive (Figure 14d−f) at room temperature. The SEM images (Figure 14a,d) were used to analyze the wear mechanism. For all test conditions, it was found that the dominant types of wear were the abrasive wear and material smearing. The material smearing is typically caused by the plastic deformation during the sliding contact, while the abrasive wear is developed by the contact induced shear stress. The MGO used in experiments is comprised of molecularly thin flakes, which facilitate the tangential motion of the contacting surfaces due to the smaller interlayer shear. Even though MGO can decrease the friction as shown in Figure 11, its flakes can act as third-body particles at the interface that can cause a plowing or abrasive type of wear because of its high material strength in the plane direction. Therefore, under the MGO/IL lubrication, the surface wear of bearing steel could be explained by the combined effects of abrasion by the direct steel−steel contact, abrasion by the MGO flakes, and material smearing by the contact stress. The EDS data (Figure 14b,e) confirmed the material composition of the contact pair (440C stainless steel ball and AISI 52100 bearing steel plate). Also, element mapping for Cr (Figure 14c,f) was conducted using the backscattered electrons (BSE) image, and it was found that the big dark spots in SEM images were not contact-induced products but Cr concentration of the bearing steel.

4. CONCLUSION

Systematic experiments and material characterizations were conducted to investigate the friction and wear performance of the MGO/IL lubricant with respect to the MGO concentration and temperature. The synthesized MGO/IL lubricant was applied to the sliding contact between a stainless-steel ball and a bearing steel plate. When 0.1 wt % MGO was added to the IL, it showed a lower COF than that of the IL without MGO at both RT and 100 °C. The wear volume did not change much at RT, but it slightly decreased at 100 °C. However, when the MGO concentration increased to 0.5 wt % in the IL, it significantly increased the wear volume at RT. Therefore, from the experimental data in this study, it could be concluded that if the MGO concentration is appropriately controlled, the MGO can be an effective additive to the IL $[C_7C_1im][NTf_2]$ lubricant by decreasing the friction without sacrificing the wear performance and its benefit as a friction reducer and wear inhibitor can be further enhanced at the higher operating temperature condition.

■ ASSOCIATED CONTENT

Supporting Information

The Supporting Information is available free of charge at https://pubs.acs.org/doi/10.1021/acsaenm.2c00177.

Nuclear magnetic resonance (NMR) spectra of $[C_7C_1im][NTf_2]$ and ILC_9-COOH, synthesis process of GO and RGO, dispersion quality of GO and MGO in IL, turbidity of GO/IL and MGO/IL mixtures, viscosity measurement of the IL $[C_7C_1im][NTf_2]$ and 0.1 wt % MGO/IL, thermogravimetric analysis (TGA) data for neat IL and the 0.1 wt % MGO/IL mixture, Raman spectroscopy of GO and MGO, experimental setup and procedures for tribotests, and calculation of nominal contact pressure and Stribeck number (PDF)

■ AUTHOR INFORMATION

Corresponding Author

Chang-Dong Yeo − *Department of Mechanical Engineering, Texas Tech University, Lubbock, Texas 79409, United States;* orcid.org/0000-0001-6489-2173; Phone: +1 806 834 5452; Email: changdong.yeo@ttu.edu

Authors

Sujoy Talukder − *Department of Mechanical Engineering, Texas Tech University, Lubbock, Texas 79409, United States*

Jagdeep Kaur − *Department of Chemistry & Biochemistry, Texas Tech University, Lubbock, Texas 79409, United States*

Jeremy Lawerence − *Department of Chemistry & Biochemistry, Texas Tech University, Lubbock, Texas 79409, United States*

Jiahe Xu − *Department of Chemistry & Biochemistry, Texas Tech University, Lubbock, Texas 79409, United States*

Ramesh Dinesh Choudhary − *Department of Mechanical Engineering, Texas Tech University, Lubbock, Texas 79409, United States*

Carol Korzeniewski − *Department of Chemistry & Biochemistry, Texas Tech University, Lubbock, Texas 79409, United States;* orcid.org/0000-0003-3672-0731

Edward L. Quitevis − *Department of Chemistry & Biochemistry, Texas Tech University, Lubbock, Texas 79409, United States;* orcid.org/0000-0002-5617-7652

Complete contact information is available at: https://pubs.acs.org/10.1021/acsaenm.2c00177

Author Contributions

The manuscript was written through contributions of all authors. All authors have given approval to the final version of the manuscript.

Notes

The authors declare no competing financial interest.

■ ACKNOWLEDGMENTS

Except for NSF (CBET-1922956) funding to C.K. for the Raman microscope, this research received no external funding. We thank Dr. Gordon Christopher for the use his rheometer in performing the viscosity measurements.

REFERENCES

(1) Holmberg, K.; Andersson, P.; Erdemir, A. Global energy consumption due to friction in passenger cars. *Tribiol. Int.* **2012**, *47*, 221−234.

(2) Rudnick, L. R.*Lubricant Additives - Chemistry and Applications*; CRC Press: Boca Raton, FL, U.S.A., 2003.

(3) Li, Y.; Zhao, J.; Tang, C.; He, Y.; Wang, Y.; Chen, J.; Mao, J.; Zhou, Q.; Wang, B.; Wei, F.; Luo, J.; Shi, G. Highly Exfoliated Reduced Graphite Oxide Powders as Efficient Lubricant Oil Additives. *Advanced Materials Interfaces* **2016**, *3*, 1600700.

(4) Kinoshita, H.; Nishina, Y.; Alias, A.; Fujii, M. Tribological properties of monolayer graphene oxide sheets as water-based lubricant additives. *Carbon* **2014**, *66*, 720−723.

(5) Guo, Y.-B.; Zhang, S.-W. The Tribological Properties of Multi-Layered Graphene as Additives of PAO2 Oil in Steel-Steel Contacts. *Lubricants* **2016**, *4*, 30.

(6) Wu, P.; Chen, X.; Zhang, C.; Luo, J. Synergistic tribological behaviors of graphene oxide and nanodiamond as lubricating additives in water. *Tribiol. Int.* **2019**, *132*, 177−184.

(7) Song, H. J.; Wang, Z. Q.; Yang, J. Tribological properties of graphene oxide and carbon spheres as lubricating additives. *Applied Physics A-Materials Science & Processing* **2016**, *122*, 933.

(8) Liñeira del Rio, J. M.; López, E.; Fernández, J.; García, F. Tribological properties of dispersions based on reduced graphene oxide sheets and trimethylolpropane trioleate or PAO 40 oils. *J. Mol. Liq.* **2019**, *274*, 568−576.

(9) Lee, C.; Wei, X.; Kysar, J.; Hone, J. Measurement of the elastic properties and intrinsic strength of monolayer graphene. *Science* **2008**, *321*, 385−388.

(10) Du, J. H.; Cheng, H. M. The Fabrication, Properties, and Uses of Graphene/Polymer Composites. *Macromol. Chem. Phys.* **2012**, *213*, 1060−1077.

(11) Sharma, N.; Sharma, V.; Vyas, R.; Kumari, M.; Kaushal, A.; Gupta, R.; Sharma, S. K.; Sachdev, K. A new sustainable green protocol for production of reduced graphene oxide and its gas sensing properties. *Journal of Science: Advanced Materials and Devices* **2019**, *4*, 473−482.

(12) Ye, C. F.; Liu, W.; Chen, Y.; Yu, L. Room-temperature ionic liquids: a novel versatile lubricant. *Chem. Commun.* **2001**, *21*, 2244−2245.

(13) Armand, M.; Endres, F.; MacFarlane, D.; Ohno, H.; Scrosati, B. Ionic-liquid materials for the electrochemical challenges of the future. *Nat. Mater.* **2009**, *8*, 621−629.

(14) Welton, T. Room-temperature ionic liquids. Solvents for synthesis and catalysis. *Chem. Rev.* **1999**, *99*, 2071−2083.

(15) Hagiwara, R.; Ito, Y. Room temperature ionic liquids of alkylimidazolium cations and fluoroanions. *J. Fluorine Chem.* **2000**, *105*, 221−227.

(16) Earle, M. J.; Seddon, K. R. Ionic liquids. Green solvents for the future. *Pure Appl. Chem.* **2000**, *72*, 1391−1398.

(17) Bhushan, B.; Palacio, M.; Kinzig, B. AFM-based nano-tribological and electrical characterization of ultrathin wear-resistant ionic liquid films. *J. Colloid Interface Sci.* **2008**, *317*, 275−287.

(18) Minami, I. Ionic Liquids in Tribology. *Molecules* **2009**, *14*, 2286−2305.

(19) Wu, J.; Lu, X.; Feng, X.; Shi, Y. Halogen-free ionic liquids as excellent lubricants for PEEK-stainless steel contacts at elevated temperatures. *Tribiol. Int.* **2016**, *104*, 1−9.

(20) Palacio, M.; Bhushan, B. A Review of Ionic Liquids for Green Molecular Lubrication in Nanotechnology. *Tribol. Lett.* **2010**, *40*, 247−268.

(21) Lhermerout, R.; Diederichs, C.; Perkin, S. Are Ionic Liquids Good Boundary Lubricants? A Molecular Perspective. *Lubricants* **2018**, *6*, 9.

(22) Somers, A.; Howlett, P.; MacFarlane, D.; Forsyth, M. A Review of Ionic Liquid Lubricants. *Lubricants* **2013**, *1*, 3−21.

(23) Ohtani, H.; Ishimura, S.; Kumai, M. Thermal Decomposition Behaviors of Imidazolium-type Ionic Liquids Studied by Pyrolysis-Gas Chromatography. *Anal. Sci.* **2008**, *24*, 1335−1340.

(24) Battez, A. H.; González, R.; Viesca, J. L.; Blanco, D.; Asedegbega, E.; Osorio, A. Tribological behaviour of two imidazolium ionic liquids as lubricant additives for steel/steel contacts. *Wear* **2009**, *266*, 1224−1228.

(25) Wang, H. Z.; Lu, Q.; Ye, C.; Liu, W.; Cui, Z. Friction and wear behaviors of ionic liquid of alkylimidazolium hexafluorophosphates as lubricants for steel/steel contact. *Wear* **2004**, *256*, 44−48.

(26) Vallejo, J.; Liñeira del Río, J.; Fernández, J.; Lugo, L. Tribological performance of silicon nitride and carbon black Ionanofluids based on 1-ethyl-3-methylimidazolium methanesulfonate. *J. Mol. Liq.* **2020**, *319*, 114335.

(27) Avilés, M.; Saurín, N.; Sanes, J.; Carrión, F.; Bermúdez, M. D. Ionanocarbon Lubricants. The Combination of Ionic Liquids and Carbon Nanophases in Tribology. *Lubricants* **2017**, *5*, 14.

(28) Saurín, N.; Avilés, M.; Espinosa, T.; Sanes, J.; Carrión, F.; Bermúdez, M.; Iglesias, P. Carbon nanophases in ordered nanofluid lubricants. *Wear* **2017**, *376−377*, 747−755.

(29) Pamies, R.; Aviles, M.; Arias-Pardilla, J.; Espinosa, T.; Carrion, F.; Sanes, J.; Bermúdez, M. D. Antiwear performance of ionic liquid + graphene dispersions with anomalous viscosity-temperature behavior. *Tribiol. Int.* **2018**, *122*, 200−209.

(30) Khare, V.; Pham, M.; Kumari, N.; Yoon, H.; Kim, C.; Park, J.; Ahn, S. Graphene-Ionic Liquid Based Hybrid Nanomaterials as Novel Lubricant for Low Friction and Wear. *ACS Appl. Mater. Interfaces* **2013**, *5*, 4063−4075.

(31) Saurín, N.; Sanes, J.; Bermúdez, M. New graphene/ionic liquid nanolubricants. *Materials Today: Proceedings* **2016**, *3*, S227−S232.

(32) Liu, Y.; Yu, S.; Shi, Q.; Ge, X.; Wang, W. Graphene-Family Lubricant Additives: Recent Developments and Future Perspectives. *Lubricants* **2022**, *10*, 215.

(33) Liu, Y.; Ge, X.; Li, J. Graphene lubrication. *Applied Materials Today* **2020**, *20*, 100662.

(34) Liu, L.; Zhou, M.; Mo, Y.; Bai, P.; Wei, Q.; Jin, L.; You, S.; Wang, M.; Li, L.; Chen, X.; Li, X.; Tian, Y. Synergistic lubricating effect of graphene/ionic liquid composite material used as an additive. *Friction* **2021**, *9*, 1568−1579.

(35) Fan, X.; Wang, L. High-performance lubricant additives based on modified graphene oxide by ionic liquids. *J. Colloid Interface Sci.* **2015**, *452*, 98−108.

(36) Gan, C.; Liang, T.; Li, W.; Fan, X.; Zhu, M. Amine-terminated ionic liquid modified graphene oxide/copper nanocomposite toward efficient lubrication. *Appl. Surf. Sci.* **2019**, *491*, 105−115.

(37) Gan, C.; Liang, T.; Li, W.; Fan, X.; Li, X.; Li, D.; Zhu, M. Hydroxyl-terminated ionic liquids functionalized graphene oxide with good dispersion and lubrication function. *Tribiol. Int.* **2020**, *148*, 106350.

(38) Sanes, J.; Aviles, M.; Saurín, N.; Espinosa, T.; Carrion, F.; Bermúdez, M. Synergy between graphene and ionic liquid lubricant additives. *Tribiol. Int.* **2017**, *116*, 371−382.

(39) Zheng, W.; Mohammed, A.; Hines, L. G.; Xiao, D.; Martinez, O. J.; Bartsch, R. A.; Simon, S. L.; Russina, O.; Triolo, A.; Quitevis, E. L. Effect of Cation Symmetry on the Morphology and Physicochemical Properties of Imidazolium Ionic Liquids. *J. Phys. Chem. B* **2011**, *115*, 6572−6584.

(40) Tao, R.; Tamas, G.; Xue, L.; Simon, S. L.; Quitevis, E. L. Thermophysical Properties of Imidazolium-Based Ionic Liquids: The Effect of Aliphatic versus Aromatic Functionality. *J. Chem. Eng. Data* **2014**, *59*, 2717−2724.

(41) Xue, L.; Gurung, E.; Tamas, G.; Koh, Y. P.; Shadeck, M.; Simon, S. L.; Maroncelli, M.; Quitevis, E. L. Effect of Alkyl Chain Branching on Physicochemical Properties of Imidazolium-Based Ionic Liquids. *J. Chem. Eng. Data* **2016**, *61*, 1078−1091.

(42) Marcano, D. C.; Kosynkin, D.; Berlin, J.; Sinitskii, A.; Sun, Z.; Slesarev, A.; Alemany, L.; Lu, W.; Tour, J. Improved synthesis of graphene oxide. *ACS Nano* **2010**, *4*, 4806−4814.

(43) Sengupta, I.; Chakraborty, S.; Talukdar, M.; Pal, S.; Chakraborty, S. Thermal reduction of graphene oxide: How temperature influences purity. *J. Mater. Res.* **2018**, *33*, 4113−4122.

https://doi.org/10.1021/acsaenm.2c00177
ACS Appl. Eng. Mater. XXXX, XXX, XXX−XXX

(44) Abu-Reziq, R.; Wang, D.; Post, M.; Alper, H. Platinum nanoparticles supported on ionic liquid-modified magnetic nanoparticles: Selective hydrogenation catalysts. *Advanced Synthesis & Catalysis* **2007**, *349*, 2145−2150.
(45) He, T. X.; Qingwen, D.; Wei, H.; Xiaolei, W. Colloidal suspension of graphene oxide in ionic liquid as lubricant. *Appl. Phys. A: Mater. Sci. Process.* **2018**, *124*, 777.
(46) Xue, L.; Gurung, E.; Tamas, G.; Koh, Y. P.; Shadeck, M.; Simon, S. L.; Maroncelli, M.; Quitevis, E. L. Effect of Alkyl Chain Branching on Physicochemical Properties of Imidazolium-Based Ionic Liquids. *J. Chem. Eng. Data* **2016**, *61*, 1078−1091.
(47) Vogel, H. Das Temperatur-abhängigkeitsgesetz der Viskosität von Flüssigkeiten. *Phys. Z.* **1921**, *22*, 645−646.
(48) Fulcher, G. S. Analysis of Recent Measurements of the Viscosity of Glasses. *J. Am. Ceram. Soc.* **1925**, *8*, 339−355.
(49) Compton, O. C.; Dikin, D.; Putz, K.; Brinson, C.; Nguyen, S. Electrically Conductive "Alkylated" Graphene Paper via Chemical Reduction of Amine-Functionalized Graphene Oxide Paper. *Adv. Mater.* **2010**, *22*, 892−896.
(50) Lavin-Lopez, M.d.P.; Romero, A.; Garrido, J.; Sanchez-Silva, L.; Valverde, J. Influence of Different Improved Hummers Method Modifications on the Characteristics of Graphite Oxide in Order to Make a More Easily Scalable Method. *Ind. Eng. Chem. Res.* **2016**, *55*, 12836−12847.
(51) Guerrero-Contreras, J.; Caballero-Briones, F. Graphene oxide powders with different oxidation degree, prepared by synthesis variations of the Hummers method. *Mater. Chem. Phys.* **2015**, *153*, 209−220.
(52) Korzeniewski, C.; Kitt, J. P.; Bukola, S.; Creager, S. E.; Minteer, S. D.; Harris, J. M. Single Layer Graphene for Estimation of Axial Spatial Resolution in Confocal Raman Microscopy Depth Profiling. *Anal. Chem.* **2019**, *91*, 1049−1055.
(53) Korzeniewski, C.; Peterson, E. M.; Kitt, J. P.; Minteer, S. D.; Harris, J. M. Adapting confocal Raman microscopy for in situ studies of redox transformations at electrode-electrolyte interfaces J. *Electroanal. Chem.* **2021**, *896*, 115207.
(54) Wang, Y.; Alsmeyer, D. C.; McCreery, R. L. Raman spectroscopy of carbon materials: Structural Basis of Observed Spectra. *Chem. Mater.* **1990**, *2*, 557−563.
(55) López-Díaz, D.; López Holgado, M. L.; García-Fierro, J. L.; Velázquez, M. M. Evolution of the Raman Spectrum with the Chemical Composition of Graphene Oxide. *J. Phys. Chem. C* **2017**, *121*, 20489−20497.
(56) Claramunt, S.; Varea, A.; Lopez-Diaz, D.; Velazquez, M. M.; Cornet, A.; Cirera, A. The Importance of Interbands on the Interpretation of the Raman spectrum of Graphene Oxide. *J. Phys. Chem. C* **2015**, *119*, 10123−10129.
(57) Ryu, S. H.; Shanmugharaj, A. M. Influence of Long-Chain Alkylamine-Modified Graphene Oxide on the Crystallization, Mechanical and Electrical Properties of Isotactic Polypropylene Nanocomposites. *Chem. Eng. J.* **2014**, *244*, 552−560.
(58) Zhang, T.; Zhu, G.-Y.; Yu, C.-H.; Xie, Y.; Xia, M.-Y.; Lu, B.-Y.; Fei, X.; Peng, Q. The UV Absorption of Graphene Oxide is Size-Dependent: Possible Calibration Pitfalls. *Microchimica Acta* **2019**, *186*, 207.
(59) Aguilar, G.; Mazzamaro, G.; Rasberger, M.Oxidative Degradation and Stabilisation of Mineral Oil-Based Lubricants. In *Chemistry and Technology of Lubricants*; Mortier, R., Fox, M., Orszulik, S., Eds.; Springer: Dordrecht, 2010.
(60) Zhou, F.; Liang, Y.; Liu, M. Ionic liquid lubricants: designed chemistry for engineering applications. *Chem. Soc. Rev.* **2009**, *38*, 2590−2599.
(61) https://www.machinerylubrication.com/Read/475/oil-breakdown.
(62) Lee, J.; Yeo, C.-D.; Hu, Z.; Thalangama-Arachchige, V.; Kaur, J.; Quitevis, E.; Kumar, G.; Koh, Y.; Simon, S. Friction and Wear of Pd-Rich Amorphous Alloy (Pd43Cu27Ni10P20) with Ionic Liquid (IL) as Lubricant at High Temperatures. *Metals* **2019**, *9*, 1180.
(63) Lee, J.; He, M.; Yeo, C.-D.; Kumar, G.; Hu, Z.; Quitevis, E.; Thalangama-Arachchige, V. Friction and Wear of Pd-rich Amorphous Alloy ($Pd_{43}Cu_{27}Ni_{10}P_{20}$) under Dry and Ionic Liquid (IL) Lubricated Conditions. *Wear* **2018**, *408−409*, 190.
(64) Nyberg, E.; Mouzon, J.; Grahn, M.; Minami, I. Formation of Boundary Film from Ionic Liquids Enhanced by Additives. *Applied Science* **2017**, *7*, 433.
(65) Komaba, M.; Kondo, S.; Suzuki, A.; Kurihara, K.; Mori, S. The Effect of Temperature on Lubrication Property with MoDTC-Containing Lubricant: Temperature Dependence of Friction Coefficient and Tribofilm Structure. *Tribology Online* **2018**, *13*, 275.

https://doi.org/10.1021/acsaenm.2c00177
ACS Appl. Eng. Mater. XXXX, XXX, XXX−XXX